

Original Article

# Iris Verification Using Optimized SVM, Ensemble, KNN, and NN Feature Classifiers on Selected DWT and Gabor Features Using mRMR, $\chi^2$ , ANOVA and Kruskal-Wallis Ranking Techniques

Sayan Das<sup>1</sup>, Biswajit Kar<sup>2</sup>

<sup>1,2</sup>Department of Instrumentation Engineering, Central Institute of Technology, Kokrajhar, Assam, India.

<sup>1</sup>Corresponding Author : [sayan.eie@gmail.com](mailto:sayan.eie@gmail.com)

Received: 13 September 2025

Revised: 15 October 2025

Accepted: 14 November 2025

Published: 29 November 2025

**Abstract** - The iris verification is now one of the accurate biometric verification methods because of the uniqueness of the iris structure and durable patterns of the iris. It stays consistent over time. Several distinct features can be extracted from the iris crypt and furrow patterns. In this study, iris features extracted using DWT and Gabor kernels are combined. Four feature ranking techniques are used to select the most relevant features, including Chi-square ( $\chi^2$ ), Minimum Redundancy Maximum Relevance (mRMR), Kruskal-Wallis tests, and Analysis of Variance (ANOVA). The top-ranked features are identified as the global features. Using them, the verification accuracy was evaluated using Discriminant Analysis, k-Nearest Neighbours (KNN), Ensemble Methods, Naive Bayes Classifiers, Support Vector Machines (SVM), and Neural Networks (NN) separately. The SVM, Ensemble, KNN, and NN models were then optimized through a hyperparameter-tuned Bayesian optimizer. A comparison of the verification performance of these machine learning methods was studied. It is found that the experimental results show excellent verification accuracies for the optimized classification models: SVM (94.1%), KNN (93.9%), Ensemble Methods (85.6%), and Neural Networks (88.3%). These findings highlight the importance of feature selection and model optimization in improving the classification models, such as SVM, Ensemble, KNN, and NN, for iris verification. The optimized SVM achieved the highest verification accuracy on the UBIRIS iris database. This result surpasses some previous studies. So, this research provides valuable insights that improve the accuracy and efficiency of an iris verification system.

**Keywords** - Bayesian optimization, DWT, Gabor, Feature ranking, Iris.

## 1. Introduction

Iris is a complex mesh of connective tissue, often referred to as the human barcode. The area between the pupil and the sclera is called the iris. Iris verification is considered an efficient technique due to its long-lasting and unique features; even identical twins do not share the same iris patterns. Iris recognition systems are widely used in biometric identification and verification for their high accuracy and reliability [1].

Considering the iris pattern as a reliable physiological characteristic in a biometric verification system for individuals, extensive research continues in this area. This system includes four main components: image capture, feature extraction, template creation, and matching. It remains challenging to extract distinct iris features achieved from their intricate patterns, such as crypts, furrows, rings, and freckles. It has been observed that various well-known methods,

including DWT, DCT, FFT, and Gabor, have been used separately in different studies for feature extraction. A gap is also found in determining the ranking of these features and the verification accuracies achieved using different classification models.

In this study, the UBIRIS Iris database, comprising 239 individuals with five iris images each, was used for the experiment. After segmenting the iris from the eye images, features were extracted using the discrete wavelet transform and Gabor kernels. Then, a novel approach has been taken by fusing the features achieved and ranking them using mRMR, Chi-square, ANOVA, and Kruskal-Wallis methods to conduct a comprehensive analysis and identify the most distinctive features. Finally, iris classification and verification were performed using several machine learning models, including Discriminant Analysis, K-Nearest Neighbours (KNN), Ensemble methods, Naive Bayes, Support Vector Machines (SVM), and Neural Networks, to determine the most effective



model for the analysis. The optimization algorithm is applied to analyze the improvement in verification accuracy.

## 2. Related Work

The article by Ohmaid et al. describes a segmentation algorithm for eye regions, utilising edge detection and the Hough Transform to identify the pupil and iris. They have normalized the iris shape, applied discrete wavelet transformation for size reduction, and employed the URIBIS database for user verification with KNN or SVM classifiers based on the iris code [2]. Narote et al. developed a system using dual-tree complex wavelet transform. They achieved high accuracy in iris recognition and demonstrated strong capabilities for both acceptance and rejection [3]. Khoje et al. extracted the iris features from the iris images available in the UBIRIS database using the wavelet transform technique. They normalized the data and used PCA to reduce the dimensionality of the data. They perform the feature classification using the combination of two well-known classifiers, i.e. support vector machines and decision trees and achieved good results [4]. Boateng et al. did a comparative study of the performance of four classification algorithms: KNN, SVM, RF, and NN. They reviewed 68 articles and textbooks published between 2000 and 2017. They compared the accuracy, robustness, stability, sensitivity, and noise sensitivity of all these models. They also assessed the model's capability for handling large datasets, data fitting, and tuning time and identified the top-performing algorithm by analyzing their performance, strengths, and weaknesses [5]. Tahir and Anghelus used Gabor kernels with specific orientations to extract iris features. They then combined these features into a single image, which they had used for matching. They performed iris localization, eyelid removal, and Hamming distance matching methods and developed an iris recognition system. They utilised CASIA-1, CASIA-Lamp-4, and SDUMLA-HMT databases. Their system achieved an accuracy of 98.85% on the CASIA-1 database [6]. Kumar et al. did a comparative study on iris recognition. They extracted the iris features using DCT, Haar wavelet, Log-Gabor, and FFT. They then performed a comparison study of iris authentication using those features. They found that the Haar wavelet and Log-Gabor filter-based phase encoding methods produce the best results among the four methods they examined [7]. Bhadra et al. did a comparative study of five supervised feature selection methods (VWMMR, INMIFS, DFS, mRMR and SVM-RFE-CBR) for multi-omics datasets. They measured the classification accuracy using four classifiers, including Naive Bayes, C4.5, AdaBoost and KNN. They identified the signature genes for specific disease omic data, facilitating an understanding of higher-order feature dependencies [8]. Putri et al. employed feature selection to enhance performance, which they evaluated using a 10-fold cross-validation. They also assessed the confusion matrix and ROC curves. They studied 500 positive and 500 negative reviews as training data. They achieved 93.10% accuracy in PSO-based Naive Bayes with an AUC of 0.750. The PSO-

based SVM achieved 91.30% accuracy with an AUC of 0.970. They classified Naive Bayes as Fair, and SVM as excellent with respect to the accuracy [9]. Zhang et al. highlighted that selecting the correct algorithm is crucial for biomedical researchers tackling practical problems. They studied seven advanced algorithms, including SVM, C4.5, AdaBoost, KNN, Naive Bayes, random forest, and logistic regression. They applied them to twelve popular UCI datasets for classification. They compared the algorithms' performances based on the results [10].

Moyasar Therar et al. named their system IRISNet. They used a convolutional neural network to extract features and a softmax layer to classify them. They evaluated on the IITD V1 iris database and achieved identification rates of 97.32% and 96.43% for original and normalised images, respectively [11]. Mehrotra et al. extracted iris texture by dividing the total iris into four segments that were usually not occluded by eyelashes. They extracted the features using the Speeded-Up Robust Features (SURF) technique [12]. El-Sofany et al. proposed an iris recognition method that uses unique iris patterns, extracting features with Hamming Distance (HD) and CNN. They tested on the MMU, IITD, and CASIA Iris datasets, which achieved recognition rates of 99.50%, 97.18%, and 95.07%, respectively [13]. A study by Chen et al. found that the improved PCHIP-LMD algorithm achieved a 78% recognition rate, which is lower than the 92% achieved by the CNN algorithm [14]. Alwawi and Althabhawee collected, pre-processed, and augmented the iris dataset using techniques like HE and CLAHE. They extracted the features using a CNN with layers that included convolution, ReLU, pooling, fully connected, and SoftMax for classification into N classes. Trained with backpropagation and Adam on a GPU in MATLAB, their model achieved 95.33% accuracy in 17.59 minutes and 100% accuracy in 12 seconds [15].

Yin, Yimin et al. summarized 120 papers on iris recognition with deep learning, covering its background, motivation, key datasets, and tasks like identification, segmentation, presentation attack detection, and localization [16]. Zanolensi et al. specifically proposed VGG and ResNet-50 architectures for processing iris images with or without segmentation and normalization. They employed transfer learning from the face domain and introduced a data augmentation technique tailored for iris images. Their results showed that non-normalized, circle-delimited iris images achieve a new state of the art in the NICE II protocol, a subset of the UBIRIS database known for challenging unconstrained images. They reported an average EER of 13.98% [17]. Sallam et al. used a Convolutional Neural Network (CNN) model to perform feature extraction and classification of the CASIA-V1 and ATVS datasets. They achieved identification rates of 98% and 97.83%, respectively [18]. Minaee et al. investigated the use of deep features from VGG-Net for iris recognition. They tested it on two well-known iris databases,

and their experiments achieved good results with an accuracy of 99.4% [19].

### 3. Materials and Methods

In this section, the iris verification system has been discussed. The flowchart of the proposed system is shown in Figure 1. The first task is to acquire the eye image and preprocess it for further processing.

The iris is then segmented and normalized for feature extraction. After extracting the iris features, the most distinct features are selected based on their ranking using ranking algorithms. Different classification algorithms are applied to classify the top-ranked features and compared.

#### 3.1. Image Acquisition and Preprocessing

At first, the iris of a person is captured using specialized cameras [20]. These cameras use infrared during capture. Infrared illumination highlights the iris pattern and also minimizes reflections and shadows.

Then this image is fed to the preprocessing stages, where necessary steps are taken to make it sufficient for further analysis. In this step, noise reduction, contrast enhancement, and normalisation of image illumination are also performed [21, 22].

#### 3.2. Iris Segmentation and Normalization

In this step, the iris region is located and segmented. The circular Hough transform is used to detect the outer and inner boundaries of the iris. This doughnut-shaped iris is normalized to Cartesian form using Daugman's rubber sheet model [21, 23].

#### 3.3. Feature Extraction

In this experiment, the iris features are extracted using a combination of the Discrete Wavelet Transform (DWT) and Gabor wavelets. Discrete Wavelet Transform (DWT) decomposes the iris image into different frequency sub-bands, including approximation, horizontal, vertical, and diagonal details [24]. This decomposition captures the texture and edge information. The coefficients extracted from the chosen sub-bands act as unique features of the iris. By convolving the iris image with Gabor kernels at multiple scales and orientations, essential features such as ridges, edges, and intensity variations are extracted [25]. The resulting Gabor coefficients form a feature vector that uniquely represents the iris pattern.

The convolution kernel can be expressed as shown in Equation (1) :

$$G(m,n;\lambda,\theta,\psi,\sigma,\gamma)=\exp\left(-\frac{m'^2+\gamma^2n'^2}{2\sigma^2}\right)\exp\left[i\left(2\pi\frac{m'}{\lambda}+\psi\right)\right] \quad (1)$$

Where,  $m' = m \cos \theta + n \sin \theta$

$n' = -m \sin \theta + n \cos \theta$

$\lambda$ =sinusoidal factor wavelength,

$\theta$ = normal to parallel stripes of Gabor function orientation,

$\psi$ = phase offset,

$\gamma$ = spatial aspect ratio,

and  $\sigma$ = standard deviation of Gaussian envelope.

#### 3.4. Feature Ranking and Selection

The obtained iris features are ranked using four feature ranking algorithms, and the top-ranked features are selected from them. These four feature selection algorithms are discussed in the following section.

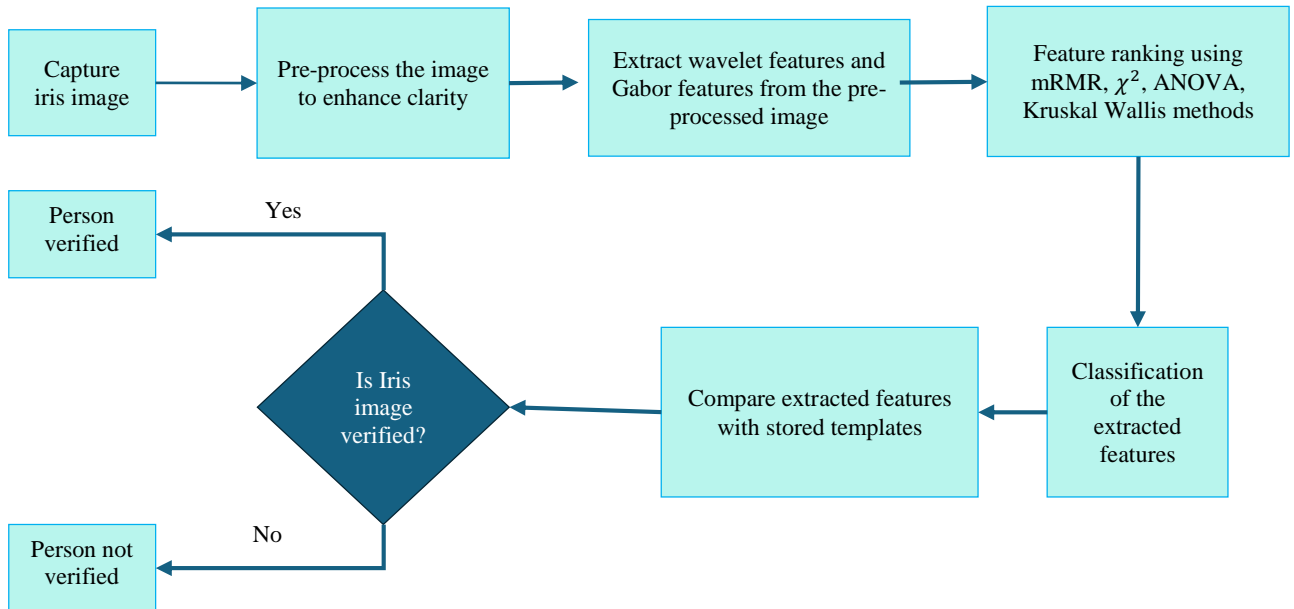


Fig. 1 The flowchart of the Iris verification process

### 3.4.1. Minimum Redundancy Maximum Relevance (mRMR)

The mRMR feature selection method selects features that are highly relevant to the target variable while minimizing redundancy among them. [26]. It ensures that the selected features offer highly relevant information about the iris pattern.

### 3.4.2. Chi-Square ( $\chi^2$ )

The  $\chi^2$  statistic evaluates the individuality between categorical features and the target variable [27]. Features with higher chi-square values are deemed more significant for classification.

This ranks features based on their  $\chi^2$  statistic, which measures the independence of two events. This measures the relationship between the features and the target variable as shown in Equation (2).

$$\chi^2 = \sum \frac{(O_f - E_f)^2}{E_f} \quad (2)$$

Where  $O_f$  = observed frequency and  $E_f$  = expected frequency

### 3.4.3. Analysis of Variance (ANOVA)

ANOVA tests for significant differences between groups of features based on their mean values [28]. By comparing the variance within groups to the variance between groups, ANOVA detects features that most effectively differentiate different iris patterns. ANOVA can be expressed using Equation (3).

$$F = \frac{\text{Mean sum square between groups}}{\text{Mean sum of squares for Error}} \quad (3)$$

### 3.4.4. Kruskal-Wallis Test

This is a non-parametric method used to determine whether multiple groups differ significantly based on their feature values. [29]. It is appropriate for ranking features when the data distribution does not meet the assumptions of parametric tests. The test statistics can be expressed in Equation (4).

$$H = (N_T - 1) \frac{\sum_{k=1}^{gp} n_k (\bar{r}_{k\cdot} - \bar{r})^2}{\sum_{k=1}^{gp} \sum_{l=1}^{n_k} (\bar{r}_{kl} - \bar{r})^2} \quad (4)$$

Where,  $N_T$  is the total observations across groups,  
 $gp$  is the group value and  $n_k$  is observations in  $k$  group,  
 $r_{kl}$  is the rank of observation  $k$  from the  $l$  group,  
 $\bar{r}_{k\cdot}$  is the average rank of all group  $k$  observations,  
 $\bar{r}$  is the average of all  $r_{kl}$ .

By employing these feature ranking techniques, the most informative global features are selected, thereby enhancing the performance of classification models, including SVM, KNN, Ensemble, Neural networks, Naive Bayes, and logistic regression.

### 3.5. Feature Classification

The selected iris features are classified using various models, including logistic regression, Naive Bayes, SVM, KNN, Ensemble Methods, and Neural Networks. Based on the similarity scores and pre-defined thresholds, the system makes a verification decision. If the score exceeds the threshold, the iris is considered a match; otherwise, it is rejected.

## 4. Results and Discussion

The UBIRIS iris database is a publicly available dataset widely used in iris recognition research [30]. It comprises images collected under various conditions to replicate real-world scenarios, including different lighting environments and factors that introduce noise. The UBIRIS database contains a total of 239 subjects.

For each subject, five iris images of the same eye are available. In this study, all the images are fed to the preprocessing stage of iris verification. During examination, it was found that 59 subjects did not have suitable iris images for this study.

So, a total of 180 subjects were examined, each accompanied by five images. In Table 1, the main stages in iris image processing are presented for five iris images of different persons. The details of each column of Table 1 are given below:



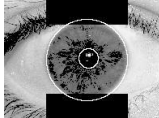
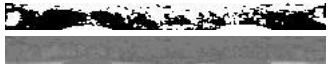






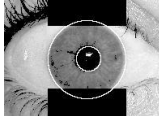
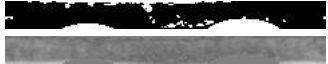

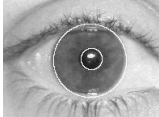
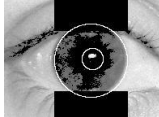
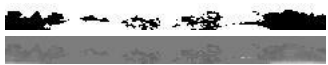




The iris image represents the raw input images of the iris. These images are first fed to the preprocessing stage for further processing. The circular boundaries of the iris and pupil are detected in the iris and pupil boundary detection step. The images shown under this column have two detected boundaries: inner and outer boundaries. The area inside these boundaries will be extracted in the later stages to extract the doughnut-shaped iris.

Accurate detection is crucial for isolating the region of interest and reducing errors in subsequent processes. The noise removal step eliminates or minimizes noises such as eyelids and eyelashes. In the normalization stage, the doughnut-shaped circular iris structure is normalized to a rectangular strip of data, shown in the 4<sup>th</sup> column of Table 1.

Further stages include classification methods such as discriminant analysis, Naïve Bayes method, SVM, neural networks, KNN, and ensemble techniques, which cannot be shown in this table. The proposed algorithm was applied to 180 subjects, and all the features are ranked using four feature ranking algorithms described in Section 3.4.

The classification models used in this analysis include Logistic Regression, Naive Bayes, Support Vector Machines (SVM), k-Nearest Neighbors (KNN), Ensemble methods, and Neural Networks. The verification accuracies were then compared for these classification models.

Table 1. Primary stages in iris image processing for biometric analysis of 5 iris images

Iris image	Iris and pupil boundary detection	Noise removal	Extracted iris after normalization
			
			
			
			
			

The primary focus was on wavelet and Gabor kernel features. The following tables, Table 2 and Table 3, provide a detailed breakdown of the 112 features, their types, and the associated operations and attributes. Out of them, 16 features are associated with wavelets. Features 1-4 are associated with the db4 wavelet. Features 5-8 are associated with Haar wavelets. Features 9-12 are associated with the coif3 wavelet. The rest of the features, features 13-16 are associated with the sym4 wavelet. These wavelets are utilized for performing the Discrete Wavelet Transform (DWT). Each wavelet feature involves operations such as calculating the mean and standard deviation of the approximation coefficients, as well as the horizontal coefficients. These coefficients are essential components in wavelet analysis. They provide valuable insights into the signal's characteristics at various levels of detail.

Table 2. DWT operation and its respective features

Feature number	Feature type	Description of features (coefficients)
F1	db4 wavelet	Mean of approximation
F2		Standard deviation of approximation
F3		Mean of horizontal
F4		Standard deviation of horizontal
F5	Haar wavelet	Mean of approximation
F6		Standard deviation of approximation
F7		Mean of horizontal
F8		Standard deviation of horizontal
F9	coif3	Mean of approximation

F10	wavelet	Standard deviation of approximation
F11		Mean of horizontal
F12		Standard deviation of horizontal
F13	sym4 wavelet	Mean of approximation
F14		Standard deviation of approximation
F15		Mean of horizontal
F16		Standard deviation of horizontal

Table 3. The Gabor kernel features used in this study

Feature name	Feature coefficients			Feature name	Feature coefficients		
	$\theta$	$\sigma$	$\lambda$		$\theta$	$\sigma$	$\lambda$
F17	$0^\circ$	1	4	F65	$90^\circ$	1	4
F18		8	8	F66		8	8
F19		2	4	F67		2	4
F20		8	8	F68		8	8
F21		4	4	F69		3	4
F22		8	8	F70		3	8
F23	$11.2^\circ$	1	4	F71	$101.25^\circ$	1	4
F24		8	8	F72		8	8
F25		2	4	F73		2	4
F26		8	8	F74		8	8
F27		4	4	F75		3	4
F28		8	8	F76		3	8
F29	$22.5^\circ$	1	4	F77	$112.5^\circ$	1	4
F30		8	8	F78		8	8
F31		4	4	F79		2	4
F32		8	8	F80		2	8

F33	33.75°	3	4	F81	123.75°	3	4
F34			8	F82		8	
F35		1	4	F83		1	4
F36	33.75°	2	8	F84		2	8
F37			4	F85			4
F38		3	8	F86		3	8
F39	45°	4	8	F87	135°	4	8
F40		1	4	F88		1	4
F41		2	8	F89		2	8
F42	56.25°	3	4	F90	146.25°	3	4
F43		4	8	F91		4	8
F44		1	4	F92		1	4
F45	67.5°	2	8	F93	157.5°	2	8
F46		3	4	F94		3	4
F47		4	8	F95		4	8
F48	78.75°	1	4	F96	168.75°	1	4
F49		2	8	F97		2	8
F50		3	4	F98		3	4
F51		4	8	F99		4	8
F52		1	4	F100		1	4
F53		2	8	F101		2	8
F54		3	4	F102		3	4
F55		4	8	F103		4	8
F56		1	4	F104		1	4
F57		2	8	F105		2	8
F58		3	4	F106		3	4
F59		4	8	F107		4	8
F60		1	4	F108		1	4
F61		2	8	F109		2	8
F62		3	4	F110		3	4
F63		4	8	F111		4	8
F64		1	4	F112		1	4
		2	8			2	8

identified as the most relevant feature, with a score of 0.831. Features 87 and 3 are scored 0.6542 and 0.0693, respectively, next in this list. This ranking indicates that Feature 93 is the most significant feature here for the model's good performance. In contrast, features lower on the list, such as Feature 55 with a score of 0.0226, have a lesser influence.

Table 4. mRMR and Chi-square ( $\chi^2$ ) feature rankings (Top 20)

mRMR			Chi-square ( $\chi^2$ )		
Rank	Feature name	Score	Rank	Feature name	Score
1	F93	0.8310	1	F93	421.7470
2	F87	0.6542	2	F97	411.3022
3	F3	0.0693	3	F45	410.1460
4	F33	0.0636	4	F37	406.6862
5	F63	0.0379	5	F43	403.2278
6	F105	0.0377	6	F91	400.9289
7	F67	0.0356	7	F9	391.7694
8	F12	0.0340	8	F13	361.2948
9	F81	0.0336	9	F5	360.1795
10	F43	0.0316	10	F1	352.3994
11	F51	0.0306	11	F49	342.4678
12	F69	0.0283	12	F85	342.4678
13	F2	0.0273	13	F51	241.9699
14	F79	0.0273	14	F87	224.3471
15	F9	0.0271	15	F10	223.3805
16	F57	0.0266	16	F2	219.5272
17	F39	0.0251	17	F6	211.8853
18	F75	0.0239	18	F39	209.9884
19	F91	0.0235	19	F99	205.4411
20	F55	0.0226	20	F8	205.2704

Following the wavelet features, the Gabor kernel features have been presented in Table 3. The parameters used here,  $\theta$ ,  $\sigma$ , and  $\lambda$ , define the orientation, scale, and frequency of the Gabor kernels. They are used to capture a wide range of texture patterns in images. For each combination of these parameters, the Gabor kernel is applied multiple times, reflecting the versatility and comprehensive nature of the analysis. The parameters include various angles  $\theta$ , such as  $0^\circ$ ,  $11.25^\circ$ ,  $22.5^\circ$ , and so on upto  $168.75^\circ$ . For each angle, there are three values of  $\sigma$ . For each  $\sigma$  value, there are two combinations of  $\lambda$  values. So, for each angle, six features are achieved. The extensive variety of angles and parameter combinations ensures that the features extracted can effectively represent the underlying structures within the data.

#### 4.1. Feature Ranking

In Table 4, the mRMR (Minimum Redundancy Maximum Relevance) features and the  $\chi^2$  features are shown. The top twenty features are listed in order of their rank. mRMR is used here to select the most significant features while eliminating redundant ones. Notably, Feature 93 is

The Chi-square ( $\chi^2$ ) feature rankings (Table 4) show the importance of different features in a dataset. Table 4 provides the top twenty  $\chi^2$  values among all features, highlighting their significance. Features with higher  $\chi^2$  values are considered more important as they indicate a stronger association with the target variable. The highest-ranked features, including Feature 93 (421.747), Feature 97 (411.3022), and Feature 45 (410.146), have the highest  $\chi^2$  values. Mid-ranked features, such as Feature 5 (360.1795) and Feature 1 (352.3994), show moderate  $\chi^2$  values. Although they are less influential than the top features, they still provide valuable information for the model. Low-rank features include Feature 99 (205.4411) and Feature 8 (205.2704), which have the lowest  $\chi^2$  values. These features significantly impact the target variable and are likely essential in predictive modelling.

The feature ranking using the ANOVA and Kruskal-Wallis method is shown in Table 5. It provides a detailed analysis of the importance of various features within a dataset, ranking them accordingly. In the table, Feature 43 ranks highest with a score of 19.0315, followed closely by Feature

91, which has a score of 18.8019. These features are likely crucial for the model's predictive ability. In contrast, features like Feature 4 and Feature 12, with scores of 1.6504 and 1.2706, respectively, have much less influence on the model.

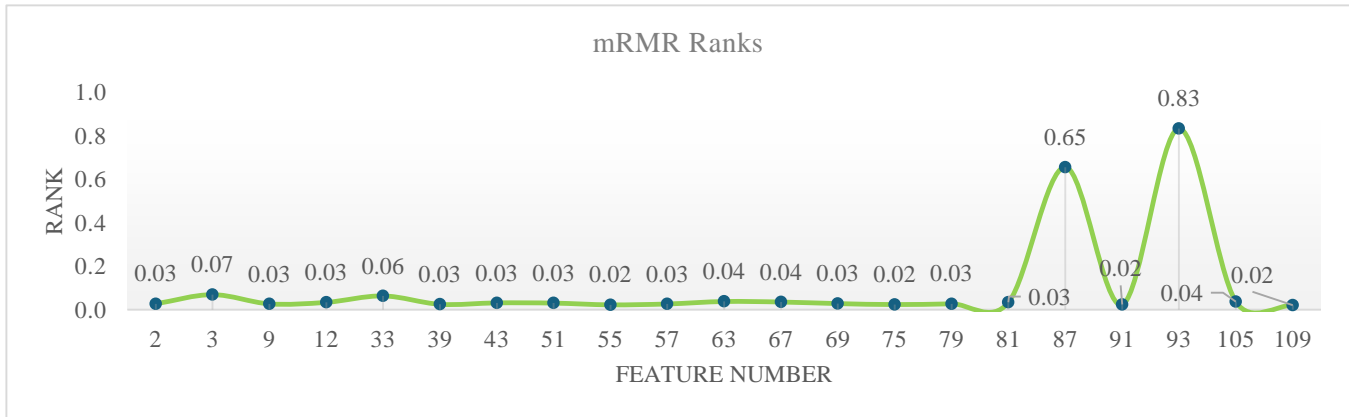
**Table 5. Feature rankings using the ANOVA and Kruskal-Wallis methods (Top 20)**

ANOVA			Kruskal-Wallis		
Rank	Feature name	Score	Rank	Feature name	Score
1	F43	19.0315	1	F1	6.25
2	F91	18.8019	2	F13	6.25
3	F9	15.2009	3	F37	6.25
4	F93	14.7293	4	F43	6.25
5	F45	14.7286	5	F45	6.25
6	F13	14.5683	6	F49	6.25
7	F1	14.5513	7	F5	6.25
8	F37	14.3670	8	F85	6.25
9	F97	14.2713	9	F9	6.25
10	F5	14.1085	10	F91	6.25
11	F49	13.3096	11	F93	6.25
12	F85	13.2895	12	F97	6.25
13	F10	10.4646	13	F10	5.79
14	F14	10.0065	14	F14	5.79
15	F2	9.8436	15	F2	5.59

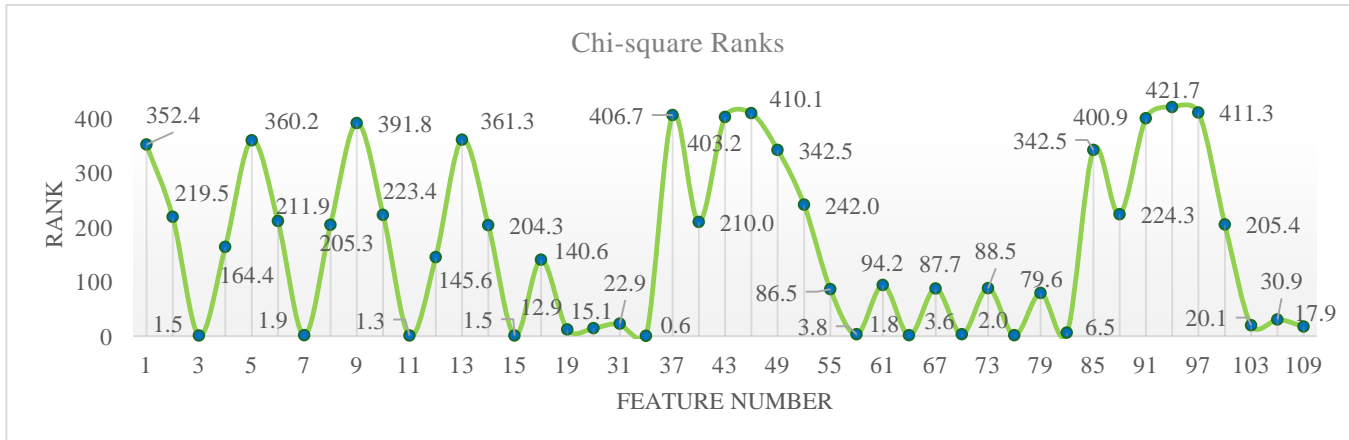
16	F6	9.4292	16	F6	5.59
17	F87	2.2746	17	F4	2.43
18	F39	2.2714	18	F12	2.17
19	F4	1.6504	19	F16	1.96
20	F12	1.2706	20	F87	1.93

The Kruskal-Wallis feature ranking (Table 5) provides an overview of the importance of various features for machine learning models. Here, 20 features, ranked by their significance, are shown. Feature 1 is the highest-ranked feature here, with a rank value of 6.25. It is observed from the table that features 1, 13, 37, 43, 45, 49, 5, 85, 9, 91, 93, and 97 are considered the most influential in the dataset. Next are Features 10 and 14, both with a rank value of 5.79, followed by Feature 2 and Feature 6 at 5.59. Moving down the list, the rank values decrease, indicating a lesser impact. Features 4 and 12 rank 2.43 and 2.17, respectively. Here, the lowest-ranked features are Feature 16 (1.96) and Feature 87 (1.93), which have minimal importance.

The following Figures 2, 3, 4, and 5 display the rankings of various distinct global features achieved by the mRMR,  $\chi^2$ , ANOVA and Kruskal-Wallis feature ranking algorithm, respectively.



**Fig. 2 mRMR feature ranking chart for various features**



**Fig. 3  $\chi^2$  ranking chart for various features**



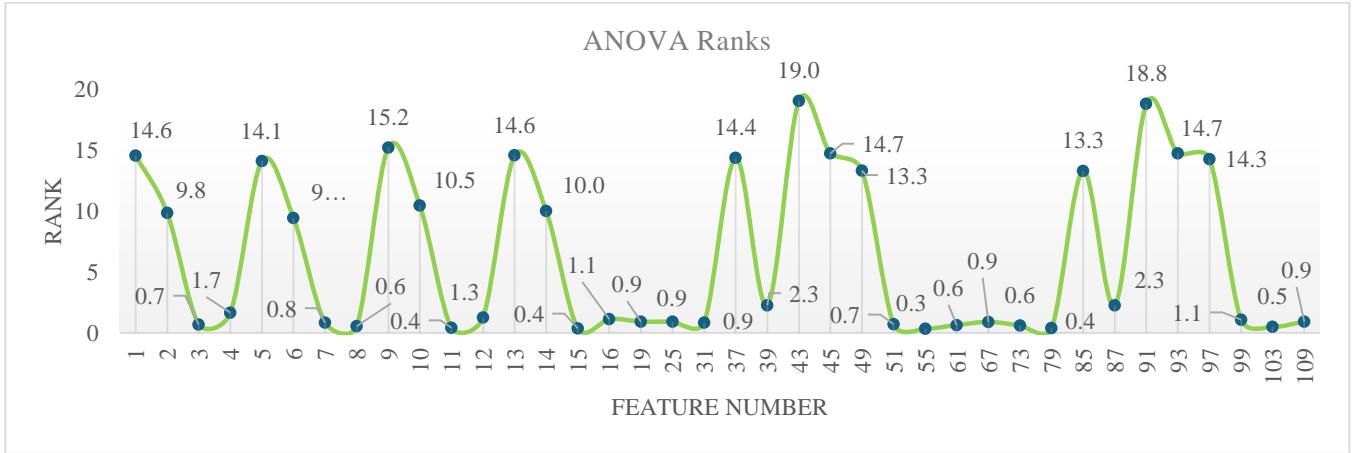


Fig. 4 ANOVA feature ranking chart for various features

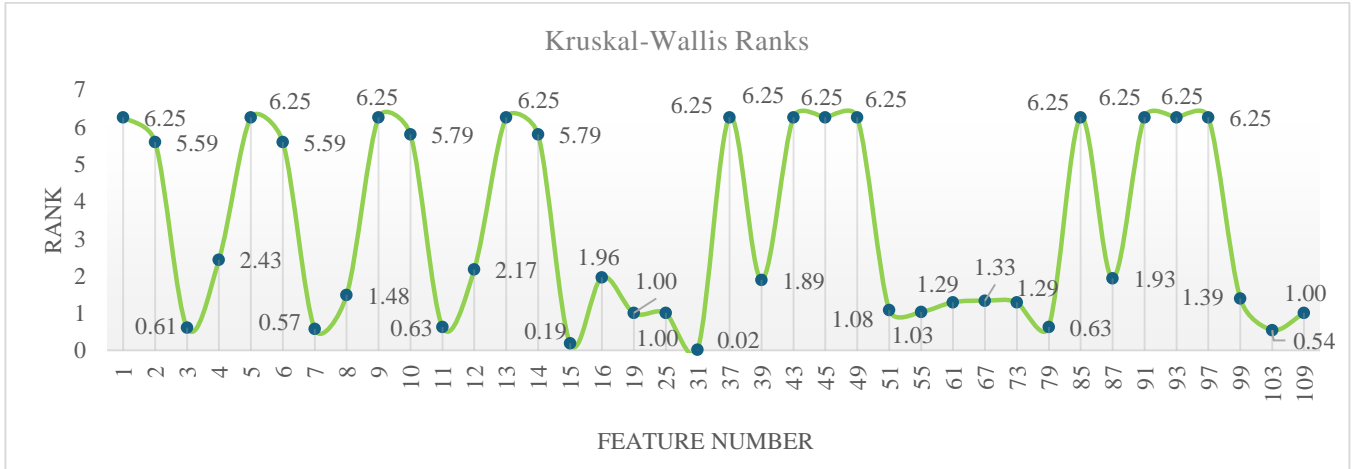


Fig. 5 Kruskal-Wallis feature ranking chart for various features

#### 4.2. Analysis of Validation Accuracy using Different Classifiers

In this study, various classifiers, including Linear Discriminant, Binary GLM Logistic Regression, Naive Bayes, SVM, KNN, Ensemble, and Neural Network, have been used for classification with different presets. In Table 6, the average verification accuracies for 180 subjects have been shown using different classification models.

##### 4.2.1. Key Findings

The Linear Discriminant classifier achieved an accuracy of 80.00%. The Binary GLM logistic regression attained an accuracy of 83.73%. The SVM model optimized with Bayesian methods achieved the highest accuracy of 94.07% among all SVM models stated. Other SVM models, including Linear, Quadratic, and Cubic, performed well, with accuracies ranging from 80.00% to 83.39%. The ensemble method that used Bayesian optimization achieved an accuracy of 85.59%, the highest among all stated ensemble models. Other ensemble models showed different performances, with Bagged Trees reaching an accuracy of 81.19% and Subspace Discriminant

reaching 84.58%. The Neural Network model with Bayesian optimization achieved the highest accuracy of 88.31% compared to all other stated Neural Network models. Other Neural Networks (Narrow, Medium, Wide, Bilayered, Trilayered) achieved accuracies ranging from 82.20% to 83.73%. The Kernel Naive Bayes performed better (78.10%) than the Gaussian Naive Bayes (72.50%). The hyperparameter settings of the Bayesian optimizer are provided in Table 7 for four classifiers.

Table 6. Analysis of testing accuracies using different classifiers

Classifier model description			Accuracy (%)
Model No.	Type	Preset	Avg.
1	Linear Discriminant		80.00
2	Binary GLM Logistic Regression		83.73
3.1	Naive Bayes	Gaussian	72.50
3.2		Kernel	78.10
4.1	SVM	Linear	80.00



4.2		Quadratic	83.90
4.3		Cubic	83.39
4.4		Fine Gaussian	76.23
4.5		Medium Gaussian	78.47
4.6		Coarse Gaussian	75.61
4.7	KNN	Bayesian optimization	94.07
5.1		Fine	81.86
5.2		Weighted	81.86
5.3	Ensemble	Bayesian optimization	93.90
6.1		Bagged trees	81.19

6.2		Subspace discriminant	84.58
6.3		Subspace KNN	85.08
6.5		Bayesian optimization	85.59
7.1		Narrow	82.20
7.2		Medium	82.71
7.3	Neural Network	Wide	83.73
7.4		Bilayered	83.56
7.5		Trilayered	82.37
7.6		Bayesian optimization	88.31

Table 7. Bayesian optimization hyperparameter settings used in the four models

Hyper-parameter configurations	SVM with Bayesian optimization	KNN with Bayesian optimization	Ensemble with Bayesian optimization	Neural network with Bayesian optimization
Optimized	Kernel: Linear Box constraint level: 1.9204	Number of neighbors: 3 Distance metric: City block Distance weight: Equal	Ensemble method: Bag Maximum number of splits: 6 Number of learners: 10 Number of predictors to sample: 66	Fully connected layers: 3 Activation function: Tanh Regularization strength (Lambda): $1.5067 \times 10^{-6}$ First layer size: 20 Second layer size: 60 Third layer size: 23
Search Ranges	Box constraint level: 0.001-1000 Kernel scale: 0.001-1000 Kernel functions: Gaussian, Linear, Quadratic, Cubic	Number of neighbors: 1-5 Distance metrics: City block, Chebyshev, Correlation, Cosine, Euclidean, Hamming, Jaccard, Mahalanobis, Minkowski (cubic), Spearman Distance weight: Equal, Inverse, Squared inverse	Ensemble method: Bag, GentleBoost, LogitBoost, AdaBoost, RUSBoost Learner range: 10-500 Rate of learning: 0.001-1 Maximum splits: 1-9 Predictors to sample: 1-112	Fully connected layers: 1-3 Activation functions: ReLU, Sigmoid, and Tanh Regularization strength (Lambda): $1 \times 10^{-6}$ First, second, and third layer size: 1-300

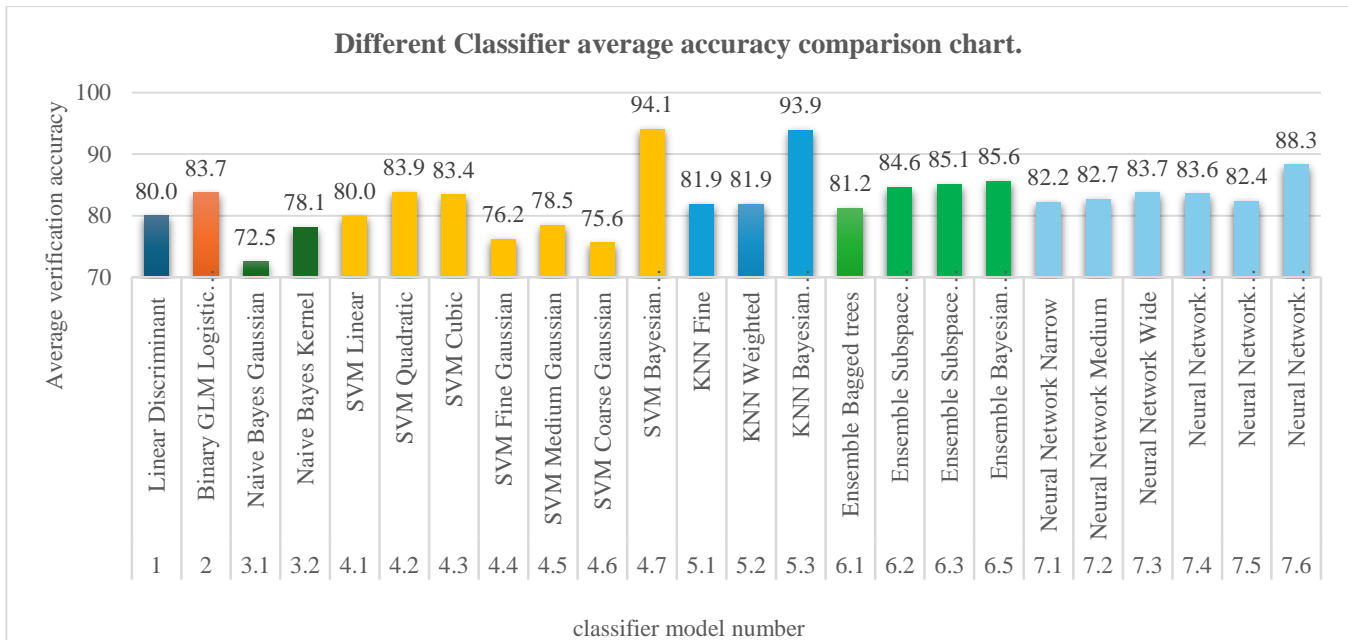


Fig. 6 Average verification accuracy comparison chart using different classification models

In summary, the classifiers, optimized using Bayesian methods, showed higher verification accuracies compared to other approaches. Among these, the Support Vector Machine (SVM) with Bayesian optimization achieved the highest accuracy at 94.07%. This was followed closely by the K-Nearest Neighbours (KNN) algorithm, which achieved an accuracy of 93.90%, and Neural Networks, which reached an accuracy of 88.31%. Meanwhile, Logistic Regression and Discriminant Analysis exhibited reasonable performance, achieving accuracies of 83.73% and 80.00%, respectively.

**Table 8. Verification accuracy comparison of the proposed method with others**

Classifier	Kernel Type	Verification accuracy(%)
<b>The method proposed by Ohmaid et al. [2] (Database used: UBIRIS)</b>		
SVM	Linear	68.2
	Quadratic	84.3
	Cubic	88.6
	Medium Gaussian	88.9
KNN	---	95.0
<b>Method proposed in this paper (Database used: UBIRIS)</b>		
SVM	Bayesian optimization	<b>94.1</b>
	Linear	80.0
	Quadratic	83.9
	Cubic	83.4
	Medium Gaussian	78.5
KNN	Bayesian optimization	93.9

Figure 6 displays the average accuracy classification analysis for all models. Discriminant Analysis, KNN, Ensemble methods, and various Neural Networks have demonstrated top performance with perfect or near-perfect accuracy. It is observed from the results that the hyper-parameter tuned Bayesian optimization has enhanced the accuracy of SVM, KNN, Ensemble methods, and Neural

Networks. This makes them highly reliable options for iris verification. However, models like Efficient Logistic Regression and specific KNN configurations underperformed and may require further optimization or reconsideration.

In this study, the Bayesian optimized SVM classifier achieved the highest verification accuracy. In Table 8, a comparison between the proposed method and the previously used method is shown. In both cases, the UBIRIS database is used. It is found that the proposed optimized SVM method outperforms the previously used methods.

## 5. Conclusion

In this experimental study, the design of a reliable and efficient iris verification system was focused on. To find out the most possible features, the DWT and Gabor features is combined. To select the most significant features among these large amounts of features, feature ranking algorithms such as mRMR, Chi-square, ANOVA, and Kruskal-Wallis are used. Different machine learning-based classifiers are then used for feature classification, and the verification accuracy is evaluated for all of them with the selected features separately. With respect to the verification accuracy, SVM, discriminant analysis, KNN, Ensemble methods, and Neural Networks scored better than the rest. The SVM, KNN, Ensemble, and Neural network models are then optimized using the Bayesian optimization technique with a set of hypertuned parameters. After optimization, the models demonstrated excellent accuracy. The SVM and KNN models achieved 94.1% and 93.9%, respectively. So, the Bayesian optimization played a vital role in improving the accuracy and reliability of the SVM, KNN, Ensemble, and Neural Network models.

## Acknowledgement

The authors thank Hugo Pedro Proença and Luís A. Alexandre from the SOCIA Lab, Soft Computing and Image Analysis Group, Department of Computer Science at the University of Beira Interior, 6201-001 Covilhã, Portugal, for providing the iris image database used in this research.

## References

- [1] Kiran B. Raja, R. Raghavendra, and Christoph Busch, "Video Presentation Attack Detection in Visible Spectrum Iris Recognition Using Magnified Phase Information," *IEEE Transactions on Information Forensics and Security*, vol. 10, no. 10, pp. 2048-2056, 2015. [[CrossRef](#)] [[Google Scholar](#)] [[Publisher Link](#)]
- [2] Hicham Ohmaid et al., "Comparison between SVM and KNN Classifiers for Iris Recognition using a New Unsupervised Neural Approach in Segmentation," *IAES International Journal of Artificial Intelligence*, vol. 9, no. 3, pp. 429-438, 2020. [[CrossRef](#)] [[Google Scholar](#)] [[Publisher Link](#)]
- [3] Sandipan P Narote et al., "An Iris Recognition based on Dual Tree Complex Wavelet Transform," *TENCON 2007 - 2007 IEEE Region 10 Conference*, Taipei, Taiwan, pp. 1-4, 2007. [[CrossRef](#)] [[Google Scholar](#)] [[Publisher Link](#)]
- [4] Suchitra Khoje, and Sanjay Mohite, "A SVM Based Iris Recognition using Wavelet Packet Transform and Manhattan Distance," *International Journal of Scientific and Technology Research*, vol. 9, no. 2, pp. 6232-6236, 2020. [[Google Scholar](#)] [[Publisher Link](#)]
- [5] Ernest Yeboah Boateng, Joseph Otoo, and Daniel A. Abaye, "Basic Tenets of Classification Algorithms K-Nearest-Neighbor, Support Vector Machine, Random Forest and Neural Network: A Review," *Journal of Data Analysis and Information Processing*, vol. 8, no. 4, pp. 341-357, 2020. [[CrossRef](#)] [[Google Scholar](#)] [[Publisher Link](#)]

- [6] Ahmed AK. Tahir, and Steluta Anghelus, "Improving Iris Recognition Accuracy Using Gabor Kernels With Near-Horizontal Orientations," *International Journal of Advances in Signal and Image Sciences*, vol. 8, no. 1, pp. 25-39, 2022. [[CrossRef](#)] [[Google Scholar](#)] [[Publisher Link](#)]
- [7] Ajay Kumar, and Arun Passi, "Comparison and Combination of Iris Matchers for Reliable Personal Authentication," *Pattern Recognition*, vol. 43, no. 3, pp. 1016-1026, 2010. [[CrossRef](#)] [[Google Scholar](#)] [[Publisher Link](#)]
- [8] Tapas Bhadra et al., "Comparison of Five Supervised Feature Selection Algorithms Leading to Top Features and Gene Signatures from Multi-Omics Data in Cancer," *BMC Bioinformatics*, vol. 23, pp. 1-18, 2022. [[CrossRef](#)] [[Google Scholar](#)] [[Publisher Link](#)]
- [9] Dwi Andini Putri et al., "Comparison of Naive Bayes Algorithm and Support Vector Machine using PSO Feature Selection for Sentiment Analysis on E-Wallet Review," *Journal of Physics: Conference Series*, vol. 1641, 2020. [[CrossRef](#)] [[Google Scholar](#)] [[Publisher Link](#)]
- [10] Yiyan Zhang et al., "Empirical Study of Seven Data Mining Algorithms on Different Characteristics of Datasets for Biomedical Classification Applications," *Biomedical Engineering Online*, vol. 16, pp. 1-15, 2017. [[CrossRef](#)] [[Google Scholar](#)] [[Publisher Link](#)]
- [11] Maryim Omran, and Ebtesam N. AlShemmary, "An Iris Recognition System Using Deep convolutional Neural Network," *Journal of Physics: Conference Series*, vol. 1530, pp. 1-12, 2020. [[CrossRef](#)] [[Google Scholar](#)] [[Publisher Link](#)]
- [12] Hunny Mehrotra et al., "An Efficient Iris Recognition using Local Feature Descriptor," *2009 16<sup>th</sup> IEEE International Conference on Image Processing (ICIP)*, Cairo, Egypt, pp. 1957-1960, 2009. [[CrossRef](#)] [[Google Scholar](#)] [[Publisher Link](#)]
- [13] Hosam El-Sofany, Belgacem Bouallegue, and Yasser M. Abd El-Latif, "A Proposed Biometric Authentication Hybrid Approach using Iris Recognition for Improving Cloud Security," *Heliyon*, vol. 10, pp. 1-16, 2024. [[CrossRef](#)] [[Google Scholar](#)] [[Publisher Link](#)]
- [14] H. Chen, and B.R. Bakshi, "Linear Approaches for Nonlinear Modeling," *Comprehensive Chemometrics*, vol. 3, pp. 453-462, 2009. [[CrossRef](#)] [[Google Scholar](#)] [[Publisher Link](#)]
- [15] Bashra Kadhim Olewi Chabor Alwawi, and Ali Fadhil Yaseen Althabhawee, "Towards More Accurate and Efficient Human Iris Recognition Model using Deep Learning Technology," *Telkommika (Telecommunication Computing Electronics and Control)*, vol. 20, no. 4, pp. 817-824, 2022. [[CrossRef](#)] [[Google Scholar](#)] [[Publisher Link](#)]
- [16] Yimin Yin et al., "Deep Learning for Iris Recognition: A Review," *Neural Computing and Applications*, vol. 37, pp. 11125-11173, 2025. [[CrossRef](#)] [[Google Scholar](#)] [[Publisher Link](#)]
- [17] Luiz A. Zanlorensi et al., "The Impact of Preprocessing on Deep Representations for Iris Recognition on Unconstrained Environments," *2018 31<sup>st</sup> SIBGRAPI Conference on Graphics, Patterns and Images (SIBGRAPI)*, Parana, Brazil, pp. 289-296, 2018. [[CrossRef](#)] [[Google Scholar](#)] [[Publisher Link](#)]
- [18] Amer Sallam et al., "Iris Recognition System Using Convolutional Neural Network," *2021 International Conference on Software Engineering & Computer Systems and 4<sup>th</sup> International Conference on Computational Science and Information Management (ICSECS-ICOCSIM)*, Pekan, Malaysia, pp. 109-114, 2021. [[CrossRef](#)] [[Google Scholar](#)] [[Publisher Link](#)]
- [19] Shervin Minaee, Amirali Abdolrashidiy, and Yao Wang, "An Experimental Study of Deep Convolutional Features For Iris Recognition," *2016 IEEE Signal Processing in Medicine and Biology Symposium (SPMB)*, Philadelphia, PA, USA, pp. 1-6, 2016. [[CrossRef](#)] [[Google Scholar](#)] [[Publisher Link](#)]
- [20] Yuqing He, Yangsheng Wang, and Tieniu Tan, "Iris Image Capture System Design for Personal Identification," *Advances in Biometric Person Authentication*, vol. 3338, pp. 539-545, 2004. [[CrossRef](#)] [[Google Scholar](#)] [[Publisher Link](#)]
- [21] J. Daugman, "How Iris Recognition Works," *IEEE Transactions on Circuits and Systems for Video Technology*, vol. 14, no. 1, pp. 21-30, 2004. [[CrossRef](#)] [[Google Scholar](#)] [[Publisher Link](#)]
- [22] John Daugman, "New Methods in Iris Recognition," *IEEE Transactions on Systems, Man, and Cybernetics, Part B: Cybernetics*, vol. 37, no. 5, pp. 1167-1175, 2007. [[CrossRef](#)] [[Google Scholar](#)] [[Publisher Link](#)]
- [23] Anil K. Jain et al., *Handbook of Biometrics*, Springer US, pp. 1-556, 2008. [[Google Scholar](#)] [[Publisher Link](#)]
- [24] P. White, "Transforms, Wavelets," *Encyclopedia of Vibration*, pp. 1419-1435, 2001. [[CrossRef](#)] [[Publisher Link](#)]
- [25] John Daugman, "Iris Encoding and Recognition using Gabor Wavelets," *Encyclopedia of Biometrics*, pp. 787-797, 2009. [[CrossRef](#)] [[Google Scholar](#)] [[Publisher Link](#)]
- [26] Hanchuan Peng, Fuhui Long, and C. Ding, "Feature Selection Based on Mutual Information: Criteria of Max-Dependency, Max-Relevance, and Min-Redundancy," *IEEE Transactions on Pattern Analysis and Machine Intelligence*, vol. 27, no. 8, pp. 1226-1238, 2005. [[CrossRef](#)] [[Google Scholar](#)] [[Publisher Link](#)]
- [27] Alisha Sikri, N.P. Singh, and Surjeet Dalal, "Chi-Square Method of Feature Selection: Impact of Pre-Processing of Data," *International Journal of Intelligent Systems and applications in Engineering*, vol. 11, no. 3s, pp. 1-8, 2023. [[Google Scholar](#)] [[Publisher Link](#)]
- [28] M.O. Arowolo et al., "A Feature Selection Based on One Way Anova For Microarray Data Classification," *Al-Hikmah Journal of Pure & Applied Sciences*, vol. 3, pp. 30-35, 2016. [[Google Scholar](#)] [[Publisher Link](#)]
- [29] William H. Kruskal, and W. Allen Wallis, "Use of Ranks in One-Criterion Variance Analysis," *Journal of the American Statistical Association*, vol. 47, no. 260, pp. 583-621, 1952. [[CrossRef](#)] [[Google Scholar](#)] [[Publisher Link](#)]
- [30] Hugo Proença, and Luís A. Alexandre, "UBIRIS: A Noisy Iris Image Database," *13<sup>th</sup> International Conference on Image Analysis and Processing - ICIAP 2005*, Cagliari, Italy, pp. 970-977, 2025. [[CrossRef](#)] [[Google Scholar](#)] [[Publisher Link](#)]